International Journal of Computer Information Systems and Industrial Management Applications
ISSN 2150-7988 Volume 18(21s) 2026 pp. 1144-1161
https://doi.org/10.70917/ijcisim-2026-5384
Article

Automated Length Measurement of Pangasius Fingerlings Using a YOLO-Assisted Vision System on Raspberry Pi

Nguyen Phuc Truong[1,2], Luong Vinh Quoc Danh1*, Nguyen Chanh Nghiem[1]

[1]College of Engineering, Can Tho University, Can Tho City, Vietnam
[2]Faculty of Electrical and Electronics Engineering, Vinh Long University of Technology Education, Vinh Long Province, Vietnam
*Corresponding author: lvqdanh@ctu.edu.vn

Abstract: Regular measurement of fish length is essential for monitoring growth performance and evaluating the health status of fish in aquaculture. Accurate length measurements provide important information for optimizing feed management and facilitating size-based grading and sorting processes. However, conventional manual measurement methods are time-consuming and may cause stress or physical injury due to repeated handling. This paper presents an automated length measurement method for Pangasius fingerlings by integrating the YOLO26n-Seg-NCNN instance segmentation model with OpenCV-based image processing techniques. The proposed approach improves the robustness of object recognition and mask extraction under varying illumination conditions, thereby enhancing the reliability of fish length estimation. Experimental results show that, compared with the conventional OpenCV-based method, the YOLO-OpenCV approach reduced the maximum absolute error from 12.12 mm to 2.71 mm, corresponding to an improvement of 9.41 mm, while increasing the minimum measurement accuracy from 90.06% to 97.41%. Furthermore, a lightweight edge-AI framework is developed by optimizing the deep learning-based image processing pipeline for deployment on resource-constrained devices, enabling automated monitoring and management of Pangasius aquaculture production.
Keywords: Computer vision, Fish length measurement, OpenCV, Pangasius, YOLO

1. INTRODUCTION

Pangasius farming plays an important role in Vietnam's freshwater aquaculture industry, particularly in the Mekong Delta region. In 2025, Pangasius export turnover reached nearly USD 2.2 billion, and Vietnam currently supplies more than 90% of the global frozen Pangasius fillet market (Phuong Linh, 2026; PV, 2025). With the continuous expansion of Pangasius production, efficient monitoring and management of fish growth have become increasingly important. In aquaculture, regular measurement of fish length is essential for evaluating growth performance and assessing fish health. Accurate length measurements provide valuable information for feed management, as well as size-based grading and sorting processes (Mingming et al., 2015). Currently, fish farms still mainly rely on manual measurement methods, such as wooden boards or acrylic rulers, to determine fish size. However, these conventional approaches are time-consuming and may cause stress or physical injury to fish due to repeated handling.

Deep learning techniques have recently emerged as powerful tools for automated image analysis and object measurement in aquaculture applications (Zhao et al., 2025). Among them, YOLO-based models have demonstrated promising performance in fish detection and morphological parameter estimation under various environmental conditions. These approaches enable fast and non-contact fish length measurement from images, providing an effective solution for intelligent aquaculture monitoring (Liu et al., 2023).

Previous studies have explored deep learning-based approaches for automated fish measurement and monitoring in aquaculture environments. An improved YOLOv5-based vision system integrated with OpenCV was developed for fish length estimation and yield prediction in cage aquaculture (Wang et al., 2024). The approach combined object detection with image-based measurement techniques to estimate fish size from camera images. Although effective for fish monitoring, the system was mainly evaluated under controlled conditions and did not consider deployment on resource-constrained edge platforms.

An underwater fish measurement framework based on YOLOv8 and a line-laser calibration technique was proposed in (Li et al., 2024). The method used YOLOv8 keypoint detection to identify fish body landmarks and applied geometric calibration to estimate real-world body dimensions. The proposed system achieved accurate fish length and width estimation with relative errors of 2.46% and 5.11%, respectively.

A FishKP-YOLOv11-based framework was developed for automated fish size and mass estimation using a stereo camera and 3D reconstruction techniques (Wang et al., 2025). The method used a lightweight YOLOv11-based keypoint detection model to identify fish body landmarks and estimate real-world dimensions from reconstructed spatial coordinates. The proposed model achieved high detection accuracy with mAP50 of 91.8% and maintained robustness under various underwater conditions.

A low-cost underwater stereo vision system using synchronized cameras, Raspberry Pi, and OpenCV-based image processing was developed for non-contact fish size measurement (Mittún et al., 2025). The system applied stereo calibration and 3D reconstruction techniques to estimate fish length and position, achieving over 95% accuracy compared with manual measurements.

However, existing approaches still face limitations in practical deployment due to their reliance on complex hardware configurations, such as laser calibration systems, stereo cameras, and GPU-based processing platforms. These requirements increase system cost and complexity, limiting their practical implementation in fish farms with resource-constrained computing environments.

In a previous study, we proposed a Pangasius fingerling length measurement method based on conventional image processing techniques using OpenCV (Truong et al., 2026). Experimental results demonstrated that the proposed method could accurately estimate fish length under controlled image acquisition conditions. However, the process of fish detection and object extraction relies on traditional image preprocessing and segmentation techniques, making the system sensitive to interference factors such as uneven body coloration, light reflections from the fish surface, and unwanted objects in the background. These factors may reduce the robustness of object detection, thereby affecting measurement accuracy and the reliable operation of the system under practical conditions.

In this study, we propose an improved Pangasius fingerling length measurement method by integrating the YOLO26n-Seg-NCNN model into the object segmentation and extraction stages while retaining the previously developed OpenCV-based length measurement algorithm. The proposed approach enhances the robustness and stability of object detection and extraction under varying image acquisition conditions by leveraging the feature-learning capability of the deep learning model, while preserving the accuracy and effectiveness of the validated measurement algorithm. Furthermore, the model is optimized for deployment on the Raspberry Pi platform, enabling practical implementation in automated monitoring and management systems for Pangasius fingerling production.

Our main contributions are summarized as follows:

1. An improved automated Pangasius fingerling length measurement approach is proposed by integrating the YOLO26n-Seg-NCNN instance segmentation model with an OpenCV-based measurement algorithm. This integration enhances the robustness of object detection and extraction, thereby enhancing the accuracy and reliability of fish length estimation.
2. A lightweight edge-AI framework is developed by optimizing the deep learning-based image processing for resource-constrained devices, enabling real-time fish recognition and length measurement on

platforms such as the Raspberry Pi and facilitating the practical deployment of AI-driven automated aquaculture management systems.

2. MATERIALS AND METHODS

2.1 System Overview

Fig. 1 presents the principle diagram of the automatic Pangasius fingerling length measurement system. The system consists of four main components: a conveyor belt for fish transportation, a sensor for fish detection, an enclosed imaging chamber to reduce external light interference, a top-mounted camera positioned perpendicular to the conveyor belt, and a fish tank. The system is implemented on a Raspberry Pi 4B kit with 8 GB RAM, which is connected to a Basler acA1300-200uc camera (Basler, Germany) for image acquisition and real-time processing.

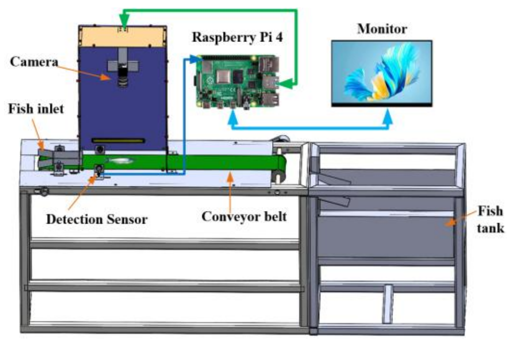

2.2 Fish Length Estimation Using YOLO26n-Seg-Based Instance Segmentation Combined with OpenCV

A. Fish Length Determination

When measuring the total fish length from the head to the end of the caudal fin, several factors may introduce measurement errors, including damage to the caudal fin during farming or transportation, as well as variations in fin posture (e.g., fully spread or folded). Some typical cases that may cause errors in total length measurement are illustrated in Fig. 2. Therefore, to ensure the accuracy of the collected data, this study defines the fish length as the distance measured from the tip of the head to the caudal peduncle (the narrowest point at the base of the tail), as illustrated in Fig. 3.

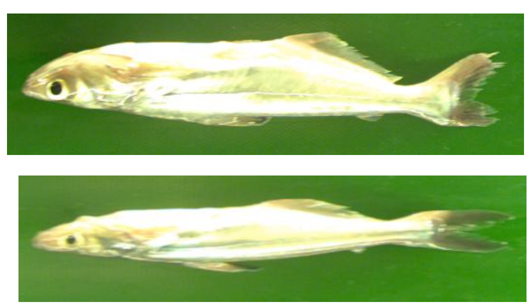

Fig. 2. Cases causing errors in total length measurement: (a) fish with a damaged caudal fin tip; (b) Fish with a folded caudal fin.

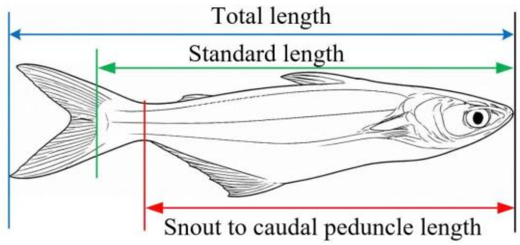

Fig. 3. Definition of fish length measurement.

B. Fish Mask Detection and Extraction Using YOLO26n-Seg Instance Segmentation

YOLO26 (or YOLOv26) represents the latest generation of real-time vision AI models developed by Ultralytics (Ultralytics, 2026). The model integrates several advanced optimization techniques to enhance computational efficiency, making it suitable for deployment on resource-constrained edge devices (Chakrabarty, 2026; Hidayatullah & Tubagus, 2026; Sapkota & Karkee, 2026). In addition, deep learning-based instance segmentation approaches, such as YOLO-Seg, have recently shown promising performance in object detection and extraction tasks with high accuracy (Xu et al., 2026).

Table 1. Distribution of the Training Dataset

	Training dataset	Validation dataset	Testing dataset
Images with fish	150	35	35
Images with no fish	32	8	8
Total	182	43	43

In our study, 268 images with size of 480x640 pixels were used for the training of the YOLO26n-Seg model. The model was trained on a laptop computer equipped with Intel Core i7-8850H CPU, 32 GB of RAM and a NVIDIA Quadro P1000 GPU with 4 GB of memory. Table 1 presents the structure of the training dataset including the image sets used for training, validation, and testing. The training set also contains 48 images captured without fish under different lighting conditions, as shown in Table 2. The model obtained after completing the training process was converted into the NCNN format (Tencent, 2026). This helps reduce the network architecture from 309 layers to 174 layers, decrease the number of parameters from 3,053,055 to 3,042,695, and reduce the computational complexity from 10.8 GFLOPs to 9.6 GFLOPs, enabling compatibility with the low-resource environment of the Raspberry Pi kit.

Table 2. Image Dataset Captured Without Fish on the Conveyor Belt

Conveyor belt condition	Illumination condition	Number of images
Dry	Low light	12
	Strong light	12
Wet	Low light	12
	Strong light	12
Total		48

3. Training Results of Fish Detection and Mask Extraction Using the YOLO26n-Seg Model

The model was fine-tuned on a Pangasius fish image dataset, where each image contains only a single fish individual, aiming to optimize the model's ability to specifically recognize and segment Pangasius fingerling objects. The dataset was divided into three subsets: training, validation, and testing, with proportions of 68%, 16%, and 16%, respectively. As shown in Fig. 4, the training results demonstrate that the F1-score reached a maximum value of 1.0

at a confidence threshold of 0.316. The recall achieved a value of 1.0 and remained stable up to a confidence threshold of 0.9. The Precision–Recall curve achieved an mAP@50 value of 0.995 (99.5%). This indicates that the model can accurately segment the location of fish in images with an Intersection over Union (IoU) above 50%. In addition, the confusion matrix results show that all 35 fish images in the validation set were correctly detected without any false positives or false negatives.

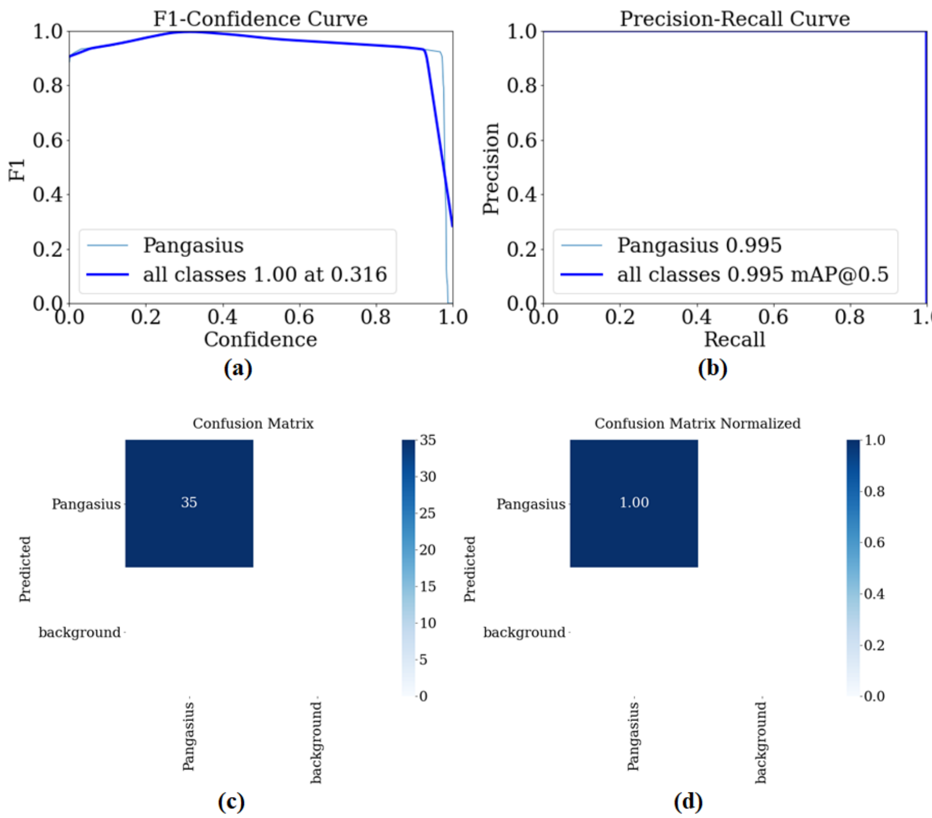

Fig. 4. Training results of the fine-tuned YOLO26n-Seg model: (a) F1-score plot; (b) Precision–Recall curve; (c) confusion matrix; (d) normalized confusion matrix.

The training process was performed using an instance segmentation model over 150 epochs. The analysis of the loss functions shows that the errors on both the training and validation sets decreased steadily and converged well, with no signs of overfitting. In addition, the Precision, Recall, and mAP50 metrics for both bounding boxes and masks exceeded 90% from the early epochs. In particular, the mAP50–95 evaluation metric continued to improve throughout the training process. This indicates that the model not only detected objects correctly and completely but also continuously refined its predictions to achieve highly accurate object mask segmentation. The results of the loss function analysis and the mAP50 and mAP50–95 metrics are presented in Fig. 5.

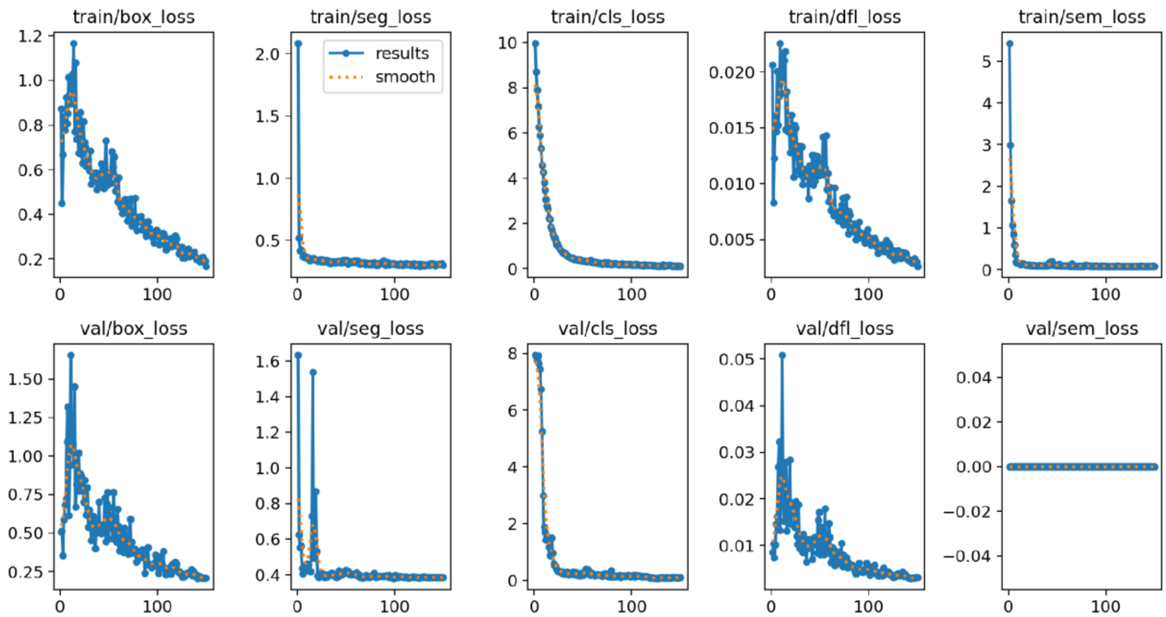

(a)

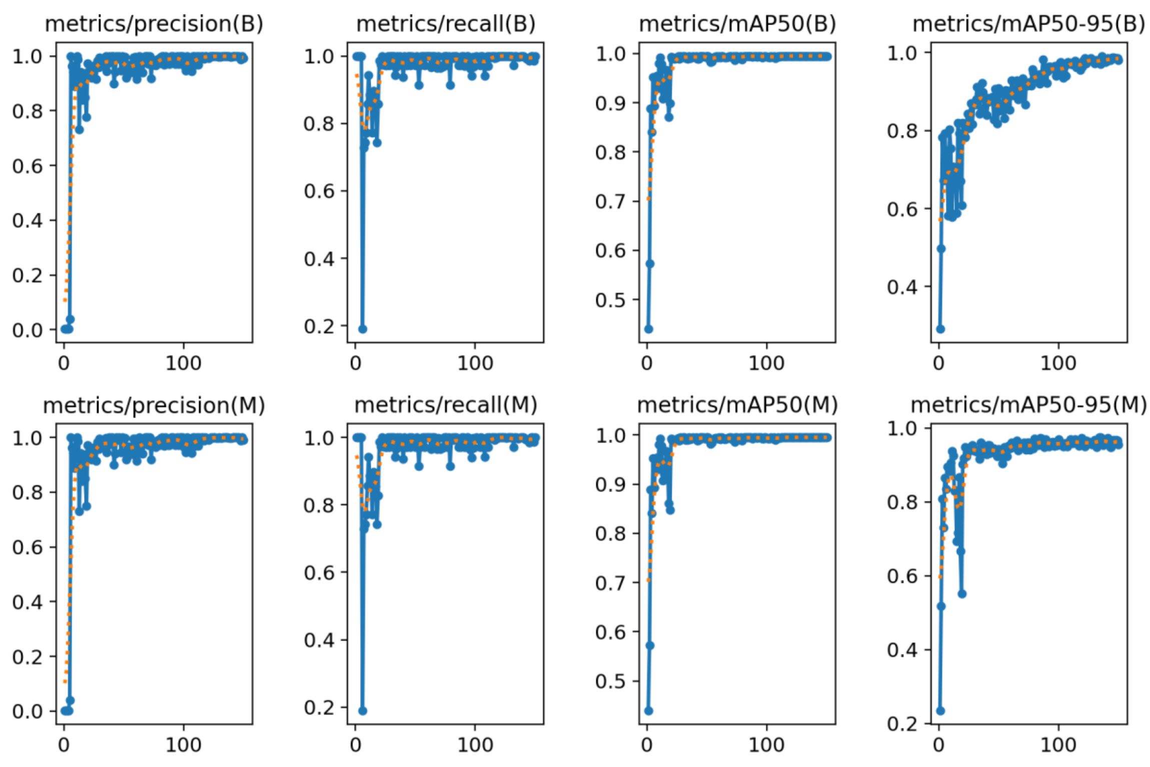

(b)

Fig. 5. Analysis results of the loss function and mAP50, mAP50-95 metrics on the training and validation datasets: (a) training set; (b) validation set.

4. Fish Length Measurement Using the YOLO-OpenCV Instance Segmentation Model

The accuracy of object detection and extraction largely depends on the quality of the captured images. Factors such as illumination conditions, light reflections on the fish body surface, distinctive dark patterns on the fish, and background noise can degrade image quality and affect detection performance. Under these conditions, conventional image preprocessing and segmentation techniques using OpenCV often suffer from low accuracy.

To overcome these limitations, this study integrates the YOLO26n-Seg model on the NCNN framework (referred to as YOLO-NCNN) for fish detection and segmentation, allowing direct extraction of object masks to support the subsequent length measurement stage. Once the object mask is obtained, OpenCV image processing algorithms are used to extract geometric features and estimate the fish length. The integration of YOLO-NCNN with OpenCV (referred to as YOLO-OpenCV) enhances the robustness of fish detection and object extraction, leading to more reliable fish length measurement results. The OpenCV-based fish length measurement algorithm was adopted from the authors' previous study to utilize the validated morphological characteristics.

Fig. 6 illustrates the workflow for image acquisition, fish detection, and length measurement based on the YOLO-OpenCV framework. Initially, the system sets up the camera configuration parameters and initializes the YOLO-NCNN model for object detection. Upon detecting a fish on the conveyor belt, the detection sensor triggers the camera to capture the image and store it in the memory. Next, the fish image is processed by the YOLO-NCNN model for object mask segmentation and extraction.

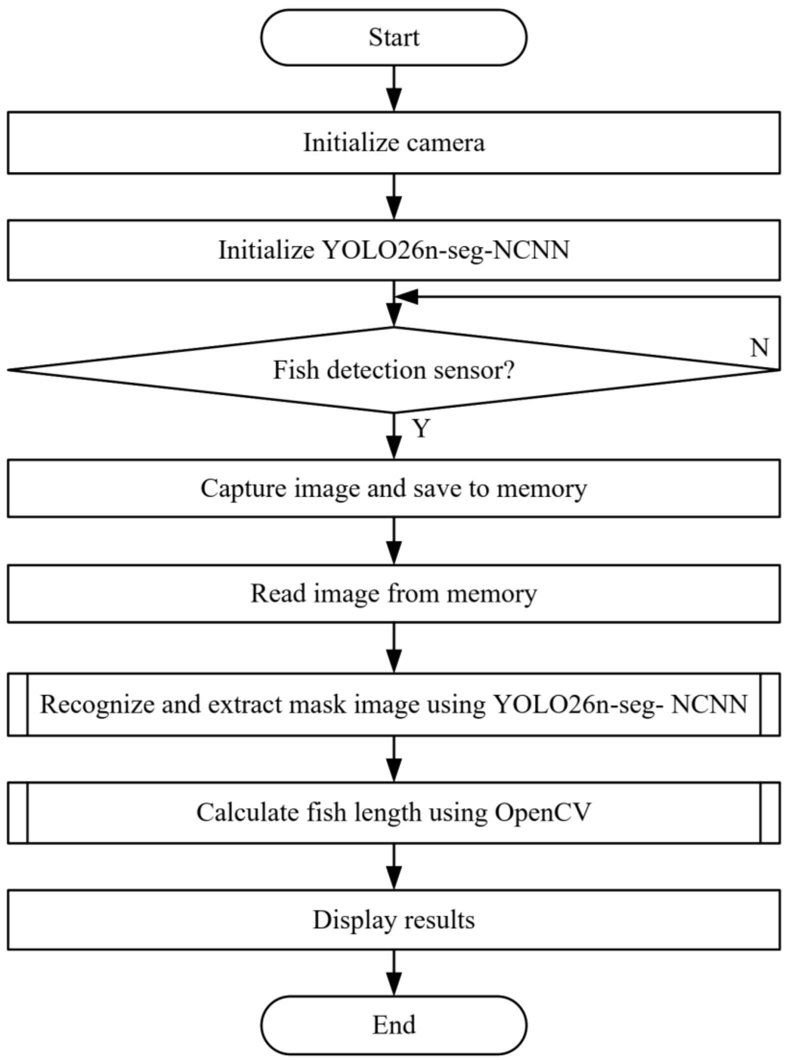

Fig. 6. Flowchart of image acquisition and processing for fish length measurement using YOLO-OpenCV model.

Finally, the fish length L (the distance from the fish head to the caudal peduncle) is estimated from the extracted mask using the OpenCV-based measurement algorithm, as shown in Fig. 7.

The fish length is determined using the following equation (Truong et al., 2026):

$$L = N * s \quad (1)$$

Where:

L: calculated fish length in millimeters.

N: the total number of image pixels located along the straight line from the fish mouth to the midpoint of the tail peduncle.

s: the physical size of a single pixel, equal to 0.264583 mm at an image resolution of 96 dpi.

Fig. 7. Fish length measurement based on the extracted mask image.

Furthermore, to minimize measurement errors caused by fish images being misaligned with the horizontal reference axis (x-axis), the image is first rotated to the standard horizontal orientation before performing the length measurement. A coordinate system xOy is then defined with its origin placed at the midpoint of the caudal peduncle, as illustrated in Fig. 8.

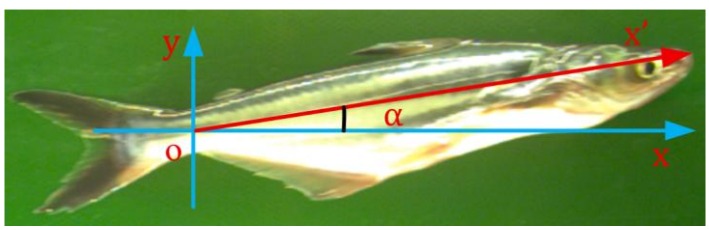

Fig. 8. Estimation of the fish orientation angle.

The longitudinal axis of the fish body (Ox') is estimated using a linear regression method based on all points belonging to the object contour. The resulting output is a direction vector:

$$v = (vx, vy) \quad (2)$$

where vx and vy represent the components of the fish body along the x-axis and y-axis, respectively. The tilt angle between the fish body axis and the horizontal reference direction is determined using the following equation (Bradski & Kaehler, 2008):

$$\alpha = 2\left(v_y, v_x\right) \times \frac{180}{\pi} \quad (3)$$

The value of α is used to generate the transformation matrix, allowing the mask image to be rotated and aligned with the horizontal reference axis.

E. Fish Length Determination Formula

In our previous study (Truong et al., 2026), the calibration relationship for the OpenCV-based measurement method was established and validated using the following equation:

$$Lop = 0.8907L + 6.975 \quad (4)$$

Where:

Lop: The estimated length from the head to the caudal peduncle using image processing.

L: The length estimated using image processing without calibration for error compensation.

The calibration equation was used to compensate for the difference between the length estimated from image processing and the actual length measured manually using a digital caliper. The OpenCV-based measurement method and the calibration relationship established in our previous study were adopted as a reference for the present study.

To establish the equation for estimating fish length using the YOLO-OpenCV method, a total of 140 Pangasius fingerlings were purchased from local fish suppliers and used in the experiments. Fish length, measured from the head to the caudal peduncle using a digital caliper with a resolution of 0.01 mm (Meterport, 2026), ranged from 79.44 to 141.90 mm, while fish weight ranged from 6.3 to 40.54 g. The measurement results are presented in Table 3, where the accuracy was calculated using the following equation:

$$Accuracy = 100 - \frac{|L_m - L_a|}{L_m} * 100 \quad (5)$$

The experimental results presented in Table 3 show that the absolute errors of the measured fish lengths ranged from 2.37 mm to 10.63 mm, with an average error of 5.69 mm. The achieved accuracy varied from 90.05% to 97.49%, resulting in an average accuracy of 94.56%.

Table 3. Comparison between manual measurement and uncalibrated YOLO-OpenCV-based measurement results

No.	**Manual measurement (mm)**	**YOLO-OpenCV** (un-calibrated, mm)	**Absolute error (mm)**	**Accuracy**	**No.**	**Manual Measurement (mm)**	**YOLO-OpenCV** (un-calibrated, mm)	**Absolute error (mm)**	**Accuracy**
	L_m	L_a	$\|L_m - L_a\|$	%		L_m	L_a	$\|L_m - L_a\|$	%
1	79.44	85.02	5.58	92.98	71	103.35	109.97	6.62	93.59
2	82.73	88.64	5.91	92.86	72	103.36	108.22	4.86	95.30
3	83.44	87.90	4.46	94.65	73	103.36	109.64	6.28	93.92
4	83.77	86.26	2.49	97.03	74	103.50	108.76	5.26	94.92
5	84.53	88.39	3.86	95.43	75	104.12	108.22	4.10	96.06
6	84.60	90.53	5.93	92.99	76	104.19	108.28	4.09	96.07
7	85.54	89.04	3.50	95.91	77	104.24	107.41	3.17	96.96
8	86.06	92.61	6.55	92.39	78	104.47	111.20	6.73	93.56
9	86.33	89.98	3.65	95.77	79	104.83	111.59	6.76	93.55
10	86.48	91.14	4.66	94.61	80	105.19	111.15	5.96	94.33
11	87.65	92.61	4.96	94.34	81	105.80	113.26	7.46	92.95
12	87.67	91.33	3.66	95.83	82	105.90	112.46	6.56	93.81
13	88.64	91.32	2.68	96.98	83	106.05	111.13	5.08	95.21
14	88.91	93.46	4.55	94.88	84	106.61	114.24	7.63	92.84
15	89.02	92.61	3.59	95.97	85	106.88	117.51	10.63	90.05
16	89.43	95.25	5.82	93.49	86	107.13	112.56	5.43	94.93
17	89.91	95.52	5.61	93.76	87	107.33	112.76	5.43	94.94
18	89.96	95.26	5.30	94.11	88	107.42	111.75	4.33	95.97
19	90.79	94.65	3.86	95.75	89	107.67	113.58	5.91	94.51
20	90.84	95.52	4.68	94.85	90	107.68	113.77	6.09	94.34
21	90.92	96.36	5.44	94.02	91	108.10	114.04	5.94	94.51
22	91.41	95.83	4.42	95.16	92	108.16	113.44	5.28	95.12
23	91.67	97.63	5.96	93.50	93	108.60	115.01	6.41	94.10

24	92.05	96.06	4.01	95.64	94	108.90	115.43	6.53	94.00
25	92.10	97.12	5.02	94.55	95	108.93	115.56	6.63	93.91
26	92.33	96.85	4.52	95.10	96	109.66	116.42	6.76	93.84
27	92.93	97.70	4.77	94.87	97	109.83	117.86	8.03	92.69
28	92.94	97.97	5.03	94.59	98	110.00	114.90	4.90	95.55
29	93.09	96.04	2.95	96.83	99	110.17	116.80	6.63	93.98
30	93.13	97.12	3.99	95.72	100	110.50	116.87	6.37	94.24
31	93.25	98.70	5.45	94.16	101	111.14	117.26	6.12	94.49
32	93.37	98.43	5.06	94.58	102	111.36	118.57	7.21	93.53
33	93.46	97.51	4.05	95.67	103	111.46	117.88	6.42	94.24
34	93.73	97.12	3.39	96.38	104	112.45	120.40	7.95	92.93
35	94.23	100.02	5.79	93.86	105	112.70	117.77	5.07	95.50
36	94.30	96.67	2.37	97.49	106	112.89	118.18	5.29	95.31
37	94.66	100.31	5.65	94.03	107	113.17	119.34	6.17	94.55
38	94.82	99.23	4.41	95.35	108	113.29	121.47	8.18	92.78
39	94.93	99.29	4.36	95.41	109	113.42	119.08	5.66	95.01
40	95.48	101.37	5.89	93.83	110	114.03	118.87	4.84	95.76
41	95.79	101.36	5.57	94.19	111	115.02	121.27	6.25	94.57
42	95.92	100.06	4.14	95.68	112	115.09	121.31	6.22	94.60
43	96.11	101.93	5.82	93.94	113	116.03	122.37	6.34	94.54
44	96.18	100.58	4.40	95.43	114	116.65	124.89	8.24	92.94
45	96.28	99.77	3.49	96.38	115	117.09	125.42	8.33	92.89
46	96.42	101.61	5.19	94.62	116	118.14	125.59	7.45	93.69
47	96.50	101.64	5.14	94.67	117	119.07	125.16	6.09	94.89
48	96.82	104.35	7.53	92.22	118	119.77	127.65	7.88	93.42
49	97.09	102.77	5.68	94.15	119	120.23	126.59	6.36	94.71
50	97.37	104.52	7.15	92.66	120	120.39	125.72	5.33	95.57
51	97.50	102.15	4.65	95.23	121	120.46	129.14	8.68	92.79
52	97.68	104.25	6.57	93.27	122	122.35	129.92	7.57	93.81
53	98.08	104.35	6.27	93.61	123	122.42	127.55	5.13	95.81
54	98.37	101.87	3.50	96.44	124	123.17	131.18	8.01	93.50
55	98.62	104.13	5.51	94.41	125	124.09	129.91	5.82	95.31
56	98.76	104.52	5.76	94.17	126	125.02	131.23	6.21	95.03
57	99.38	105.04	5.66	94.30	127	125.12	132.82	7.70	93.85
58	99.48	105.87	6.39	93.58	128	126.17	129.96	3.79	97.00
59	99.81	104.52	4.71	95.28	129	126.33	132.56	6.23	95.07
60	100.23	106.37	6.14	93.87	130	126.76	133.80	7.04	94.45
61	100.54	107.16	6.62	93.42	131	126.94	134.15	7.21	94.32
62	101.08	108.07	6.99	93.08	132	127.29	134.25	6.96	94.53
63	101.26	106.41	5.15	94.91	133	128.04	136.81	8.77	93.15
64	101.67	107.80	6.13	93.97	134	128.79	136.26	7.47	94.20
65	102.00	107.78	5.78	94.33	135	129.56	134.85	5.29	95.92
66	102.12	107.25	5.13	94.98	136	132.76	137.15	4.39	96.69
67	102.27	108.31	6.04	94.09	137	134.09	139.09	5.00	96.27
68	102.50	106.97	4.47	95.64	138	135.32	141.67	6.35	95.31
69	102.61	109.68	7.07	93.11	139	138.61	145.26	6.65	95.20
70	102.96	109.55	6.59	93.60	140	141.90	148.47	6.57	95.37

To enhance the accuracy of the automatic measurement, the MATLAB Curve Fitting Toolbox (MathWorks, 2026) was employed to establish a fish length estimation formula by calibrating the measurement errors between the manual method and the image processing-based one. The obtained linear regression model achieved a high coefficient of determination (*R2*=0.9931), as expressed in equation (6) and shown in Fig. 9.

$$L_{cal} = 0.00003624x^3 - 0.01116x^2 + 2.059x - 35.6 \qquad (6)$$

where:

Lcal: represents the calibrated fish length estimated from the head to the caudal peduncle using the YOLO-OpenCV model.

x: represents the fish length from the head to the caudal peduncle obtained from the uncalibrated image processing method.

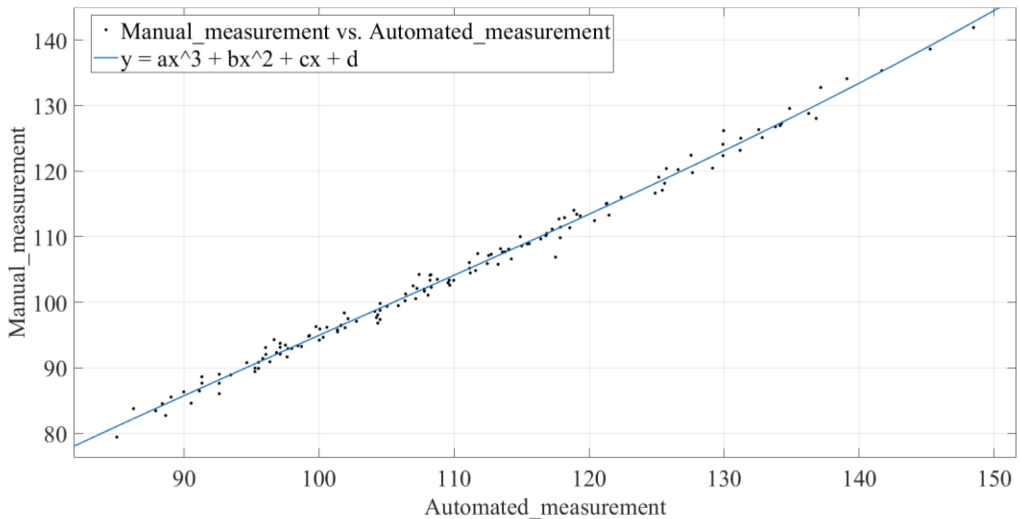

Fig. 9. Correlation analysis between manual measurements and the YOLO-OpenCV-based measurements.

The results obtained before and after applying the calibration function described in equation (6) are presented in Fig. 10. As shown in Table 4, the calibrated data demonstrate a significant improvement in the accuracy of fish length estimation.

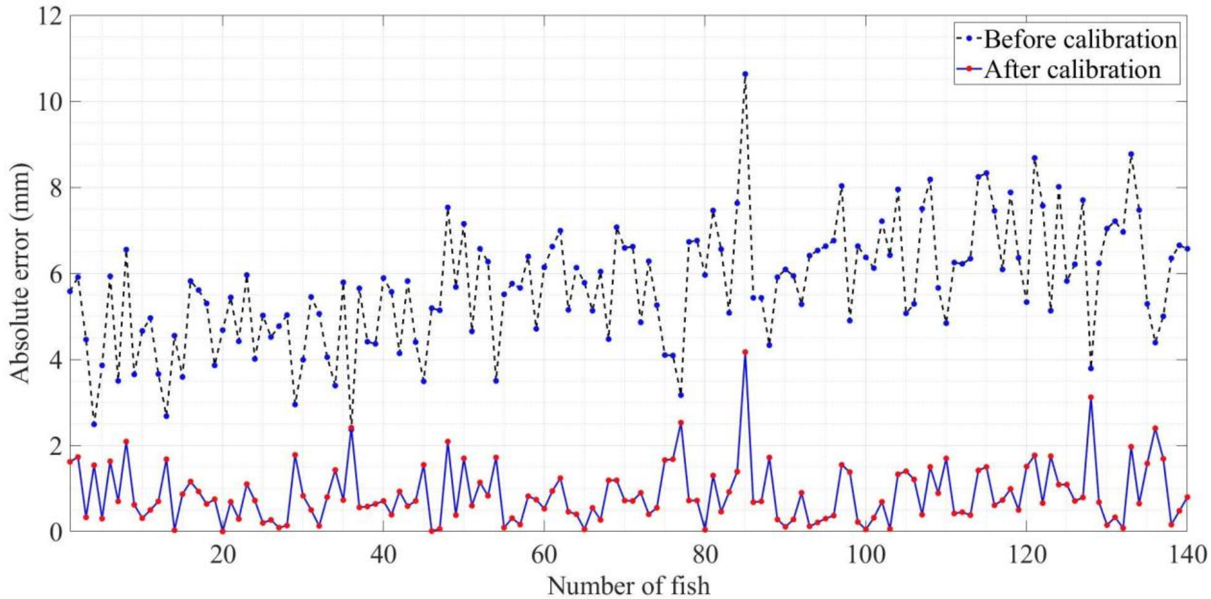

Fig. 10. Comparison of absolute errors before and after calibration.

Table 4. Comparison of Fish Length Measurement Results Before and After Calibration

	Without calibration	**With calibration**	**Notes**
Min. absolute error (mm)	2.37	0.00	Decreased by 2.37 mm
Max. absolute error (mm)	10.63	4.17	Decreased by 6.46 mm
Avg. absolute error (mm)	5.69	0.87	Decreased by 4.82 mm
Min. accuracy (%)	90.05	96.10	Increased by 6.05%
Max. accuracy (%)	97.49	100.00	Increased by 2.51%
Avg. accuracy (%)	94.56	99.16	Increased by 4.6%

5. RESULTS AND DISCUSSION

3.1 Model Validation on an Independent Dataset

To evaluate the effectiveness of the error compensation method and the stability of the YOLO-OpenCV-based measurement approach, validation experiments were conducted using 75 independent fish samples that were not included in the training or calibration datasets. The experiments focused on evaluating the method's ability to reliably detect fish and extract object masks. The fish samples had lengths ranging from 83.30 to 143.38 mm. Table 5 summarizes the fish length measurements obtained using the YOLO-OpenCV method and compares them with manual measurements. The experimental results show that the YOLO-OpenCV method achieved absolute errors ranging from 0.02 to 2.71 mm, with a mean absolute error of 0.93 mm. The measurement accuracy ranged from 97.41% to 99.98%, with an average accuracy of 99.11%.

Table 5. Validation results comparing manual measurement and YOLO-OpenCV-based measurement

No.	**Manual measurement (mm)**	**YOLO-OpenCV** (calibrated, mm)	**Absolute error (mm)**	**Accuracy**	**No.**	**Manual measurement (mm)**	**YOLO-OpenCV** (calibrated, mm)	**Absolute error (mm)**	**Accuracy**
	L_{m1}	L_{cal}	$e=\|L_{m1} - L_{cal}\|$	%		L_{m1}	L_{cal}	$e=\|L_{m1} - L_{cal}\|$	%

1	83.30	84.72	1.42	98.30	39	103.68	104.39	0.71	99.32
2	84.33	85.22	0.89	98.94	40	104.15	105.25	1.10	98.94
3	85.05	85.70	0.65	99.24	41	104.42	105.87	1.45	98.61
4	86.99	85.78	1.21	98.61	42	104.64	107.35	2.71	97.41
5	87.79	88.64	0.85	99.03	43	104.66	102.24	2.42	97.69
6	87.85	85.64	2.21	97.48	44	105.49	105.62	0.13	99.88
7	89.33	87.72	1.61	98.20	45	105.99	103.28	2.71	97.44
8	89.88	90.39	0.51	99.43	46	106.76	107.82	1.06	99.01
9	90.58	89.86	0.72	99.21	47	107.48	105.65	1.83	98.30
10	90.95	91.18	0.23	99.75	48	107.78	108.82	1.04	99.04
11	91.80	92.56	0.76	99.17	49	108.38	109.33	0.95	99.12
12	91.84	92.83	0.99	98.92	50	108.57	107.89	0.68	99.37
13	92.86	93.12	0.26	99.72	51	108.60	108.72	0.12	99.89
14	93.07	95.32	2.25	97.58	52	108.73	107.93	0.80	99.26
15	93.21	92.68	0.53	99.43	53	109.70	109.30	0.40	99.64
16	93.41	94.23	0.82	99.12	54	109.89	110.30	0.41	99.63
17	93.71	92.81	0.90	99.04	55	110.33	111.01	0.68	99.38
18	93.83	92.55	1.28	98.64	56	111.30	113.03	1.73	98.45
19	94.20	94.73	0.53	99.44	57	112.23	113.12	0.89	99.21
20	94.79	94.73	0.06	99.94	58	113.17	114.03	0.86	99.24
21	95.38	95.74	0.36	99.62	59	113.39	113.77	0.38	99.66
22	95.46	95.19	0.27	99.72	60	114.10	112.01	2.09	98.17
23	95.93	95.70	0.23	99.76	61	115.93	116.03	0.10	99.91
24	96.12	95.46	0.66	99.31	62	116.90	114.60	2.30	98.03
25	96.48	96.42	0.06	99.94	63	118.31	117.83	0.48	99.59
26	96.88	96.23	0.65	99.33	64	121.51	122.58	1.07	99.12
27	97.32	98.76	1.44	98.52	65	121.96	123.00	1.04	99.15
28	97.50	96.81	0.69	99.29	66	122.09	124.16	2.07	98.30
29	98.09	98.11	0.02	99.98	67	123.09	121.46	1.63	98.68
30	98.75	98.59	0.16	99.84	68	124.97	126.78	1.81	98.55
31	100.19	100.66	0.47	99.53	69	125.94	125.84	0.10	99.92
32	100.78	101.46	0.68	99.33	70	126.86	126.21	0.65	99.49
33	101.35	100.22	1.13	98.89	71	127.35	126.99	0.36	99.72
34	101.78	102.69	0.91	99.11	72	127.78	129.19	1.41	98.90
35	102.47	103.23	0.76	99.26	73	132.78	133.19	0.41	99.69
36	102.98	103.27	0.29	99.72	74	135.64	135.84	0.20	99.85
37	103.33	105.00	1.67	98.38	75	143.38	142.38	1.00	99.30
38	103.50	102.95	0.55	99.47					

Fig. 11 illustrates the distribution of absolute errors between the YOLO-OpenCV-based length measurements and manual measurements using the probability distribution, scatter, and cumulative distribution plots. The probability distribution plot exhibits that the majority of absolute errors are distributed within the range of 0–1.5 mm, with only a few samples showing errors greater than 2.5 mm. The scatter distribution plot shows a median error of approximately 0.76 mm, lower than the average absolute error (0.93 mm), indicating a slight skewness caused by a few samples with larger errors. The narrow interquartile range (0.41–1.26 mm) suggests low data dispersion and confirms the stability of the proposed measurement model. A small number of outliers were observed within the range of 2.5–2.71 mm; however, they had a negligible impact on the overall data distribution. The cumulative distribution plot in Fig. 11 indicates that approximately 81% of the samples achieved errors below 1.5 mm, around 90% had errors lower than 2 mm, and over 96% had errors below 2.5 mm. These results demonstrate that the majority of measurements exhibited small errors, thereby validating the high accuracy and reliability of the proposed method.

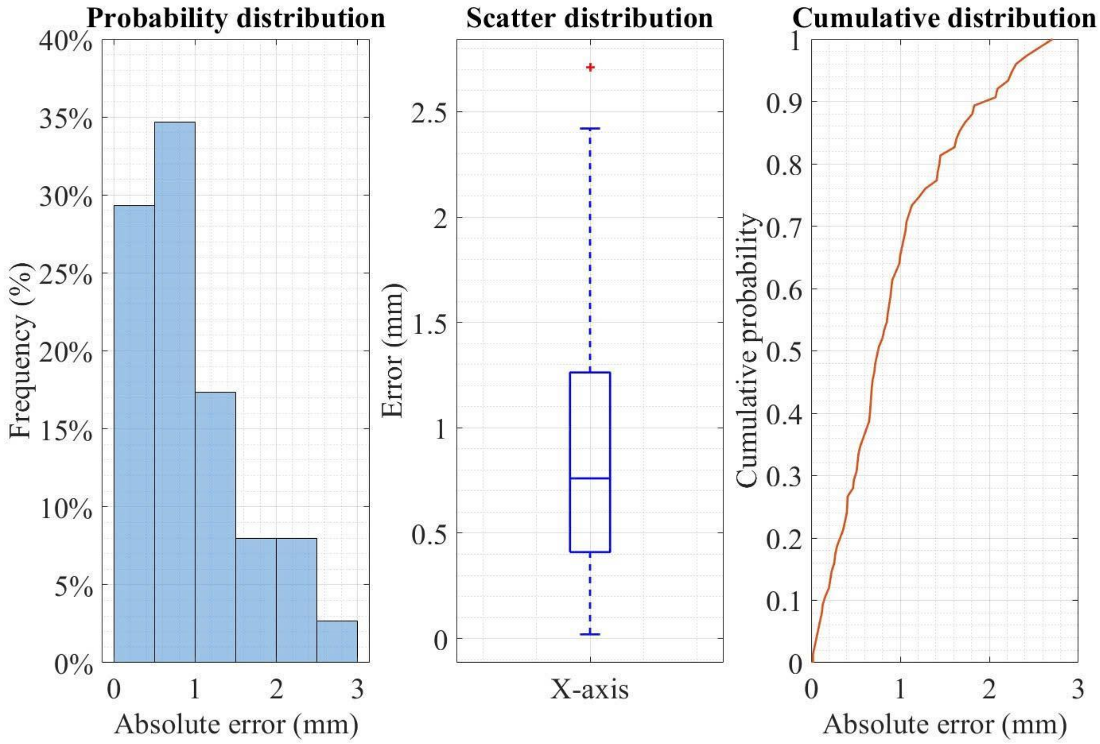

Fig. 11. Evaluation of measurement accuracy between the YOLO-OpenCV-based automatic method and manual measurement.

Furthermore, integrating the YOLO-OpenCV model for fish detection and mask extraction effectively addresses the limitations of the conventional method based solely on OpenCV. Fig. 12 illustrates a case study of mask extraction and fish length estimation results for images captured under challenging conditions caused by variations in illumination and fish body coloration. It shows that the YOLO-NCNN model can effectively detect, segment, and extract the fish mask with preserved details, allowing accurate estimation of fish length. In contrast, the conventional OpenCV-based method encountered difficulties in fully extracting the fish head region because of light scattering on the fish skin surface. The thresholding process incorrectly classified a portion of the head region as background, resulting in incomplete mask extraction and measurement errors in fish length estimation, as shown in Fig. 12(d). Specifically, the YOLO-OpenCV model achieves an absolute error of 0.69 mm, reducing the error by 8.16 mm compared with the OpenCV method (8.85 mm). In addition, YOLO-OpenCV obtains an accuracy of 99.29%, which is 8.37% higher than that of OpenCV (90.92%).

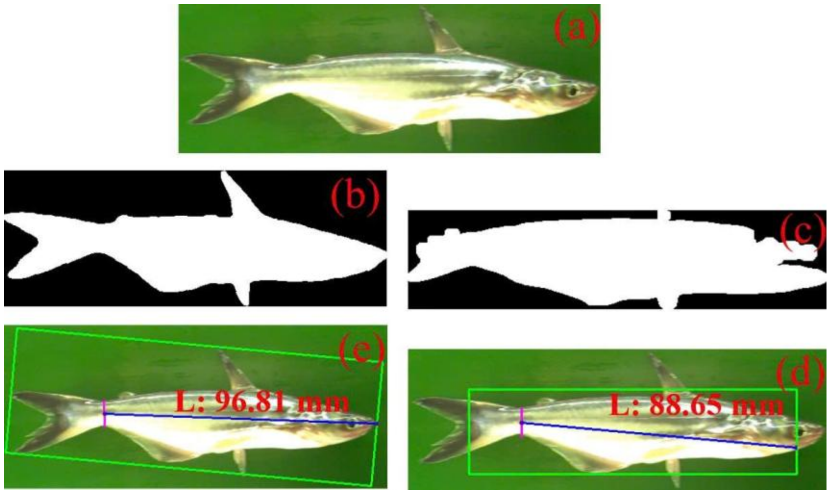

Fig. 12. Comparison of mask extraction and fish length measurement results using the YOLO-OpenCV and conventional OpenCV methods: (a) original image; (b) extracted mask using YOLO26n-Seg-NCNN; (c) extracted mask using OpenCV; (d) fish length measurement using OpenCV; (e) fish length measurement using YOLO-OpenCV.

3.2 Evaluation of the Model's Recognition Performance under Challenging Conditions

In order to further evaluate the robustness of the proposed YOLO-OpenCV method, the OpenCV-based method was also applied to the same 75 fish samples under the same lighting conditions used for evaluating YOLO-OpenCV. The light intensity was reduced by 2.7 times compared with the conditions used in the previous study, which employed only the OpenCV-based method (Truong et al., 2026). The substantial reduction in illumination decreased the amount of light reflected from the fish surface and created darker regions on the fish body. This led to the loss of important details during mask extraction, resulting in higher errors in object extraction and fish length measurement.

Table 6 presents the fish length measurement results obtained using the two methods on the same 75 samples under identical lighting conditions. The YOLO-OpenCV results in Table 6 are the same as those reported in the validation results in Table 5. Table 7 presents the absolute errors and measurement accuracy of the YOLO-OpenCV and OpenCV methods.

Table 6. Experimental Comparison Between YOLO-OpenCV and OpenCV under Challenging Lighting Conditions

No.	**Manual measurement** (mm)	**Automated measurement**		**Absolute error**		**Accuracy**		**Difference in Absolute error** (mm)
		OpenCV (mm)	YOLO-OpenCV (mm)	OpenCV (mm)	YOLO-OpenCV (mm)	OpenCV (%)	YOLO-OpenCV (%)	
	L_{m1}	L_{op}	L_{cal}	$Ab_1 = \lvert L_{m1} - L_{op} \rvert$	$Ab_2 = \lvert L_{m1} - L_{cal} \rvert$	Ac_1	Ac_2	$Ab_2 - Ab_1$
1	83.30	81.92	84.72	1.38	1.42	98.34	98.30	0.04
2	84.33	81.76	85.22	2.57	0.89	96.95	98.94	-1.68
3	85.05	77.92	85.70	7.13	0.65	91.62	99.24	-6.48
4	86.99	83.37	85.78	3.62	1.21	95.84	98.61	-2.41
5	87.79	85.53	88.64	2.26	0.85	97.43	99.03	-1.41
6	87.85	86.34	85.64	1.51	2.21	98.28	97.48	0.70
7	89.33	88.80	87.72	0.53	1.61	99.41	98.20	1.08
8	89.88	82.93	90.39	6.95	0.51	92.27	99.43	-6.44
9	90.58	81.99	89.86	8.59	0.72	90.52	99.21	-7.87
10	90.95	88.95	91.18	2.00	0.23	97.80	99.75	-1.77
11	91.80	90.66	92.56	1.14	0.76	98.76	99.17	-0.38

12	91.84	85.01	92.83	6.83	0.99	92.56	98.92	-5.84
13	92.86	89.01	93.12	3.85	0.26	95.85	99.72	-3.59
14	93.07	89.31	95.32	3.76	2.25	95.96	97.58	-1.51
15	93.21	91.77	92.68	1.44	0.53	98.46	99.43	-0.91
16	93.41	86.45	94.23	6.96	0.82	92.55	99.12	-6.14
17	93.71	84.62	92.81	9.09	0.90	90.30	99.04	-8.19
18	93.83	92.13	92.55	1.70	1.28	98.19	98.64	-0.42
19	94.20	87.83	94.73	6.37	0.53	93.24	99.44	-5.84
20	94.79	87.84	94.73	6.95	0.06	92.67	99.94	-6.89
21	95.38	93.93	95.74	1.45	0.36	98.48	99.62	-1.09
22	95.46	91.63	95.19	3.83	0.27	95.99	99.72	-3.56
23	95.93	87.12	95.70	8.81	0.23	90.82	99.76	-8.58
24	96.12	94.70	95.46	1.42	0.66	98.52	99.31	-0.76
25	96.48	94.25	96.42	2.23	0.06	97.69	99.94	-2.17
26	96.88	91.83	96.23	5.05	0.65	94.79	99.33	-4.40
27	97.32	97.98	98.76	0.66	1.44	99.32	98.52	0.78
28	97.50	88.65	96.81	8.85	0.69	90.92	99.29	-8.16
29	98.09	97.02	98.11	1.07	0.02	98.91	99.98	-1.05
30	98.75	98.02	98.59	0.73	0.16	99.26	99.84	-0.57
31	100.19	100.96	100.66	0.77	0.47	99.23	99.53	-0.30
32	100.78	99.87	101.46	0.91	0.68	99.10	99.33	-0.23
33	101.35	91.66	100.22	9.69	1.13	90.44	98.89	-8.56
34	101.78	104.15	102.69	2.37	0.91	97.67	99.11	-1.46
35	102.47	101.15	103.23	1.32	0.76	98.71	99.26	-0.56
36	102.98	96.87	103.27	6.11	0.29	94.07	99.72	-5.82
37	103.33	107.69	105.00	4.36	1.67	95.78	98.38	-2.69
38	103.50	101.14	102.95	2.36	0.55	97.72	99.47	-1.81
39	103.68	101.98	104.39	1.70	0.71	98.36	99.32	-0.99
40	104.15	101.51	105.25	2.64	1.10	97.47	98.94	-1.54
41	104.42	103.37	105.87	1.05	1.45	98.99	98.61	0.40
42	104.64	103.82	107.35	0.82	2.71	99.22	97.41	1.89
43	104.66	97.51	102.24	7.15	2.42	93.17	97.69	-4.73
44	105.49	103.36	105.62	2.13	0.13	97.98	99.88	-2.00
45	105.99	-	103.28	-	2.71	-	97.44	-
46	106.76	105.78	107.82	0.98	1.06	99.08	99.01	0.08
47	107.48	104.69	105.65	2.79	1.83	97.40	98.30	-0.96
48	107.78	105.81	108.82	1.97	1.04	98.17	99.04	-0.93
49	108.38	109.33	109.33	0.95	0.95	99.12	99.12	0.00
50	108.57	98.29	107.89	10.28	0.68	90.53	99.37	-9.60
51	108.60	108.37	108.72	0.23	0.12	99.79	99.89	-0.11
52	108.73	106.89	107.93	1.84	0.80	98.31	99.26	-1.04
53	109.70	106.49	109.30	3.21	0.40	97.07	99.64	-2.81
54	109.89	109.49	110.30	0.40	0.41	99.64	99.63	0.01
55	110.33	107.62	111.01	2.71	0.68	97.54	99.38	-2.03
56	111.30	109.49	113.03	1.81	1.73	98.37	98.45	-0.08
57	112.23	112.08	113.12	0.15	0.89	99.87	99.21	0.74
58	113.17	111.75	114.03	1.42	0.86	98.75	99.24	-0.56
59	113.39	112.32	113.77	1.07	0.38	99.06	99.66	-0.69

60	114.10	112.61	112.01	1.49	2.09	98.69	98.17	0.60
61	115.93	112.84	116.03	3.09	0.10	97.33	99.91	-2.99
62	116.90	113.70	114.60	3.20	2.30	97.26	98.03	-0.90
63	118.31	117.15	117.83	1.16	0.48	99.02	99.59	-0.68
64	121.51	119.18	122.58	2.33	1.07	98.08	99.12	-1.26
65	121.96	109.84	123.00	12.12	1.04	90.06	99.15	-11.08
66	122.09	120.12	124.16	1.97	2.07	98.39	98.30	0.10
67	123.09	120.66	121.46	2.43	1.63	98.03	98.68	-0.80
68	124.97	124.19	126.78	0.78	1.81	99.38	98.55	1.03
69	125.94	124.32	125.84	1.62	0.10	98.71	99.92	-1.52
70	126.86	123.43	126.21	3.43	0.65	97.30	99.49	-2.78
71	127.35	121.04	126.99	6.31	0.36	95.05	99.72	-5.95
72	127.78	130.53	129.19	2.75	1.41	97.85	98.90	-1.34
73	132.78	130.27	133.19	2.51	0.41	98.11	99.69	-2.10
74	135.64	134.37	135.84	1.27	0.20	99.06	99.85	-1.07
75	143.38	139.48	142.38	3.90	1.00	97.28	99.30	-2.90

Table 7. Comparison Results of the YOLO-OpenCV and OpenCV Methods

Parameters	**OpenCV** (n = 74)	**YOLO-OpenCV** (n = 75)	**Comments**
Min. absolute error (mm)	0.15	0.02	Decreased by 0.13 mm
Max. absolute error (mm)	12.12	2.71	Decreased by 9.41 mm
Avg. absolute error (mm)	3.27	0.93	Decreased by 2.34 mm
Min. accuracy (%)	90.06	97.41	Increased by 7.35%
Max. accuracy (%)	99.87	99.98	Increased by 0.11%
Avg. accuracy (%)	96.78	99.11	Increased by 2.33%

It is observable that the fish length measurement using the YOLO-OpenCV method has higher accuracy and better stability compared to the OpenCV. Although the YOLO-OpenCV model improves the average accuracy by only 2.33%, the measurement stability is significantly enhanced. The method reduces the average absolute error by 2.34 mm and increases the minimum accuracy by 7.35%.

This result also indicates that OpenCV can achieve high accuracy under strictly controlled image acquisition conditions; however, it is prone to larger errors when the image collection conditions change. Table 8 presents statistical data on cases that caused errors during mask image extraction. It can be observed that, for the OpenCV-based method, there are 36 cases where details in the mask images are lost, affecting the measurement accuracy. Among these cases, 25 occur in the head region, 3 occur in the caudal peduncle region, and 8 occur in both the head and caudal peduncle regions, accounting for 48% of the total validation samples. The errors can be attributed to the characteristically dark regions of the fish head and tail. Changes in lighting conditions can lead to misdetection in threshold-based image segmentation methods. In addition, there is one case where OpenCV failed to extract the object, resulting in an error and preventing the fish length measurement. In contrast, combining YOLO-NCNN with OpenCV improves the stability and reliability of the object recognition, extraction, and fish length measurement processes. There is only one instance of misdetection in the YOLO-OpenCV model, where the fish's whiskers randomly intersect to form a closed region in the head area, leading to an error in extracting the mask image. By learning the overall shape features of fish during the training process, the YOLO-OpenCV model can maintain stable object recognition and extraction performance even when image acquisition conditions change.

Table 8. Error Cases in the Recognition and Mask Image Extraction Stages

Cause of error	OpenCV	YOLO-OpenCV
Missing detail in the fish head area	25	0
Missing detail in the fish's caudal peduncle area	3	0
The fish's whiskers intersect to form a closed region at the head	0	1
Loss of detail in the head and tail base areas	8	0
Object could not be extracted	1	0
Total	37	1

When running on a Raspberry Pi 4B with a conveyor speed of 0.25 m/s, the use of YOLO-NCNN for image segmentation and mask extraction increased the image processing time from 0.245 to 0.647 s, corresponding to an increase of approximately 0.4 s compared with the OpenCV-based method. At this processing time, integrating YOLO-NCNN still meets the system's required throughput of approximately 3,600 fish per hour. The image processing time could be further reduced by using a Raspberry Pi 5 instead of the Raspberry Pi 4B as the computing platform.

6. CONCLUSION

This study successfully proposed and developed an automated, non-contact length measurement method for Pangasius fingerlings by integrating the YOLO-NCNN instance segmentation model with OpenCV-based image processing techniques. The proposed approach improves object recognition and mask extraction performance, particularly under image acquisition conditions with varying illumination intensity, thereby enhancing the robustness and reliability of fish length estimation.

Experimental results demonstrate that the YOLO-OpenCV approach outperforms the conventional OpenCV-based method by reducing the maximum absolute error from 12.12 mm to 2.71 mm, corresponding to an improvement of 9.41 mm, while increasing the minimum measurement accuracy from 90.06% to 97.41%. These results indicate that the proposed method effectively reduces the impact of environmental variations on the recognition process and provides more stable length measurement results. Furthermore, the optimized lightweight edge-AI framework enables real-time fish recognition and length measurement on resource-constrained devices, such as the Raspberry Pi, demonstrating its suitability for automated monitoring and management of Pangasius aquaculture production. Future work will focus on further optimizing the algorithm to improve processing speed and real-time performance. In addition, the proposed method has the potential to be adapted for other fish species with similar morphological characteristics, expanding its application in automated aquaculture systems.

REFERENCES

1. Bradski G. and Kaehler A. Learning OpenCV: Computer Vision with the OpenCV Library, 1005 Gravenstein Highway North, Sebastopol, CA 95472: O'Reilly Media, Inc., 2008, p. 577
2. Chakrabarty S., YOLO26: An Analysis of NMS-Free End to End Framework for Real-Time Object Detection. 2026; arXiv:2601.12882
3. Hidayatullah P. and Tubagus R., YOLO26: A Comprehensive Architecture Overview and Key Improvements. 2026; arXiv:2602.14582
4. Li J, Zhang S, Li P, Dai Y, Wu Z. Research on Measuring the Bodies of Underwater Fish with Inclined Positions Using the YOLOv8 Model and a Line-Laser System. Fishes. 2024; 9(6):206. https://doi.org/10.3390 /fishes9060206
5. Liu H, Ma X, Yu Y, Wang L, Hao L. Application of Deep Learning-Based Object Detection Techniques in Fish Aquaculture: A Review. Journal of Marine Science and Engineering. 2023; 11(4):867. https://doi.org /10.3390/jmse11040867
6. Mathworks. Curve Fitting Toolbox. 2026 [cited 2026 Jun 20]. https://www.mathworks.com/products/curvefitting .html
7. Meterport. (2026). *JS22F100 Electronic Digital Caliper*. Retrieved 10/08/2026 from https://meterport.com /collections/digital-caliper/products/js22f100-electronic-digital-caliper?variant=37946189807809

8. Mingming Hao, Helong Yu, Daoliang Li: The Measurement of Fish Size by Machine Vision-A Review. In: 9th International Conference on Computer and Computing Technologies in Agriculture (CCTA), Sept. 2015, pp.15-32, Beijing, China.
9. Mittún OaF, Andersen LEJ, Svendsen MBS, Steffensen JF. An Inexpensive 3D Camera System Based on a Completely Synchronized Stereo Camera, Open-Source Software, and a Raspberry Pi for Accurate Fish Size, Position, and Swimming Speed. Fishes. 2025; 10(4):139. https://doi.org/10.3390/fishes10040139
10. Phuong Linh. Pangasius exports in 2025 exceed USD 2 billion, with strong growth in multiple markets. Vietnam Association of Seafood Exporters and Producers. 2026 [cited 2026 Jun 15]. https://seafood.vasep.com.vn/key-seafood-sectors/pangasius/news/pangasius-exports-in-2025-exceed-usd-2-billion-with-strong-growth-in-multiple-markets-35925.html
11. PV. Vietnam's pangasius industry eyes high-value transformation. VietNamNet Global. 2025 [cited 2026 Jun 15]. https://vietnamnet.vn/en/vietnam-s-pangasius-industry-eyes-high-value-transformation-2421566.html
12. Sapkota R. and Karkee M., Ultralytics YOLO Evolution: An Overview of YOLO26, YOLO11, YOLOv8 and YOLOv5 Object Detectors for Computer Vision and Pattern Recognition. 2026; arXiv:2510.09653
13. Tencent. NCNN. 2026 [cited 2026 Jun 20]. https://github.com/Tencent/ncnn
14. Truong N. P., Danh L. V. Q., and Nghiem N. C. A Computer Vision-Based Method for Determining the Vaccine Injection Position in Pangasius Fingerlings. International Journal of Advanced Computer Science & Applications, vol. 17, no. 2, 2026
15. Ultralytics. The ultimate end-to-end computer vision platform. 2026. [cited 2026 Jun 19]. https://www.ultralytics.com/
16. Wang L, Chen L-Z, Peng B, Lin Y-T. Improved YOLOv5 Algorithm for Real-Time Prediction of Fish Yield in All Cage Schools. Journal of Marine Science and Engineering. 2024; 12(2):195. https://doi.org/10.3390/jmse12020195
17. Wang J, Cheng Z, Lin M, Yang R, Huang Q. FishKP-YOLOv11: An Automatic Estimation Model for Fish Size and Mass in Complex Underwater Environments. Animals. 2025; 15(19):2862. https://doi.org/10.3390/ani15192862
18. Xu, L.; Ye, H.; Wang, S.; Cao, X.; Xu, J. AquaFishNet: A Binocular Vision-Based Method for Fish Body Mass Estimation. Fishes 2026, 11, 341. https://doi.org/10.3390/fishes11060341
19. Zhao, Y., Qin, H., Xu, L. et al. A Review of Deep Learning-Based Stereo Vision Techniques for Phenotype Feature and Behavioral Analysis of Fish in Aquaculture. Artif Intell Rev 58, 7 (2025). https://doi.org/10.1007/s10462-024-10960-7